Multipoint Measurements of the Electron Jet of Symmetric Magnetic Reconnection with a Moderate Guide Field

F. D. Wilder, R. E. Ergun, S. Eriksson, T. D. Phan, J. L. Burch, N. Ahmadi, K. A. Goodrich, D. L. Newman, K. J. Trattner, R. B. Torbert, B. L. Giles, R. J. Strangeway, W. Magnes, P.-A. Lindqvist, and Yu-V. Khotyaintsev

Phys. Rev. Lett. **118**, 265101 — Published 29 June 2017

DOI: 10.1103/PhysRevLett.118.265101

Multi-point Measurements of the Electron Jet of Symmetric Magnetic Reconnection With a Moderate Guide Field

F. D. Wilder[1], R. E. Ergun[1,2], S. Eriksson[1], T. D. Phan[3], J. L. Burch[4], N. Ahmadi[1], K. A. Goodrich[1, 2], D. L. Newman[5], K. J. Trattner[1], R. B. Torbert[6], B. L. Giles[7], R. J. Strangeway[8], W. Magnes[9], P.-A. Lindqvist[10], Yu-V. Khotyaintsev[11]

[1] Laboratory of Atmospheric and Space Sciences, University of Colorado, Boulder, Colorado, 80303, USA
[2] Department of Astrophysical and Planetary Sciences, University of Colorado, Boulder, Colorado, USAe
[3] Space Sciences Laboratory, University of California, Berkeley, California, USA
[4] Southwest Research Institute, San Antonio TX, USA
[5] Department of Physics, University of Colorado, Boulder, Colorado, USA
[6] Department of Physics, University of New Hampshire, Durham, New Hampshire, USA
[7] NASA Goddard Space Flight Center, Greenbelt, MD, USA
[8] Department of Earth and Space Sciences, University of California Los Angeles, Los Angeles, California, USA
[9] Space Research Institute, Austrian Academy of Sciences, Graz, Austria
[10] Royal Institute of Technology, Stockholm, Sweden
[11] Swedish Institute of Space Physics, Uppsala, Sweden

ABSTRACT

We report observations from the Magnetospheric Multiscale (MMS) satellites of the electron jet in a symmetric magnetic reconnection event with moderate guide field. All four spacecraft sampled the ion diffusion region and observed the electron exhaust. The observations suggest that the presence of the guide field leads to an asymmetric Hall field, which results in an electron jet skewed towards the separatrix with a non-zero component along the magnetic field. The jet appears in conjunction with a spatially and temporally persistent parallel electric field ranging from -3 to -5 mV/m, which led to dissipation on the order of 8 nW/m^3. The parallel electric field heats electrons that drift through it, and is associated with a streaming instability and electron phase space holes.

I. INTRODUCTION

Magnetic reconnection is a phenomenon that can impact the behavior of heliospheric [1-7], astrophysical [8], and laboratory plasmas [9]. It changes the topology of the magnetic field and dissipates magnetic energy into particle kinetic energy and heat [10]. The mechanism by which magnetic reconnection occurs in collisionless plasmas is still not fully understood, especially on the electron scale (λ_e, the electron skin depth) [11,12]. In 2015, NASA launched the Magnetospheric Multiscale (MMS) mission to study the electron-scale physics of magnetic reconnection [13].

The first phase of the MMS mission studies magnetic reconnection on the subsolar boundary of the Earth's magnetosphere, known as the magnetopause [13]. In this region, the interplanetary magnetic field is carried by the shocked solar wind, known as the magnetosheath, to the magnetopause, where it can reconnect with the geomagnetic field. Reconnection at this current sheet is often highly asymmetric, with the plasma density in the magnetosheath being 10 times larger than in the magnetosphere [14, 15]. MMS has successfully encountered the electron diffusion region (EDR) at the dayside magnetopause multiple times [e.g. 16, 17, 18], where it has consistently observed enhanced dissipation ($\boldsymbol{J} \cdot \boldsymbol{E}'$, where $\boldsymbol{J}$ is the electric current density, $\boldsymbol{E}' = \boldsymbol{E} + \boldsymbol{V}_e \times \boldsymbol{B}$ is the electric field in the electron fluid frame, $\boldsymbol{V}_e$ is the electron bulk velocity, and $\boldsymbol{B}$ is the magnetic field)[19], as well as non-gyrotropic electron 'crescent' distributions that result from the mixing of magnetosheath and magnetospheric plasma [14, 15, 16]. A small reconnecting parallel electric field ($E_{||}$), ~3 mV/m, was also observed near the EDR.

Figure 1. MMS 1 observations from 09 December 2015 that suggest an encounter with the electron jet. (a) The ion and electron energy density, measured at a cadence of 150 and 30 ms, respectively. (b) T_i and T_e. (c) $\boldsymbol{V}_i$. (d) $\boldsymbol{V}_e$. (e) $\boldsymbol{B}$. (f) $\boldsymbol{J} = ne(\boldsymbol{V}_i - \boldsymbol{V}_e)$. (g) $E_{||}$ measured at 32 samples/s with uncertainty given in orange [22]. The perpendicular electric field, E_{perp}, is also shown in blue. (h) $\boldsymbol{J} \cdot \boldsymbol{E}'$. The LMN system is defined in the text. The vertical dashed line indicates the time when $B_L = 0$ and the vertical dotted lines indicate the interval over which minimum variance analysis was performed.

In this letter, we present MMS observations that show a crossing of the electron jet near the EDR for symmetric reconnection in the magnetosheath, as opposed to the magnetopause. The component of $\boldsymbol{B}$ out of the reconnection plane, the guide field, is approximately half of the reconnecting magnetic field. Recent simulations of moderate guide field magnetic reconnection suggest that the Hall magnetic field signatures can be skewed so that the electron jet is directed towards the separatrix, and therefore has a non-zero $\boldsymbol{V}_e$ parallel to the reconnecting field [20].

The MMS observations confirm this skewed electron jet, and show that it is coincident with a magnetic field-aligned current as well as an enduring and large scale (100s of Debye lengths) $E_{||}$ that accelerates electrons in the vicinity of the jet. The $E_{||}$ is associated with enhanced $\boldsymbol{J} \cdot \boldsymbol{E}'$, which shows that the electron jet provides extended dissipation beyond the EDR. Such a persistent $E_{||}$ structure that extends far beyond the Debye scale has never been observed in space before and appears to be sustained by a gradient in electron pressure. The electric field structure is slightly oblique to $\boldsymbol{B}$ and may act as an acceleration channel for nearby electrons.

II. OBSERVATIONS

Figure (1) shows data from MMS1 over a time span of 4s. The mission and its instruments are described in several articles [13, 21-25]. The spacecraft location (top of the figure) was in the Earth's magnetosheath near magnetic local noon. Figure (1a) shows the ion and electron number density, which remained steady between 15 and 20 cm^{-3} during most of the interval. Figure (1b) shows the parallel and perpendicular values of the electron and ion temperatures (T_i and T_e). For the interval shown in Figure 1, the observed ion and electron temperatures of a few 100 eV and a few 10 eV, respectively, are consistent with the spacecraft being in the magnetosheath, as is the number density of both species [6].

The third and fourth panels, (c) and (d), plot the ion and electron bulk velocities ($\boldsymbol{V}_i$) and ($\boldsymbol{V}_e$) in a color-coded local coordinate system labeled L, M and N. $\boldsymbol{B}$ is shown in panel (e) and is also

in LMN coordinates. The reconnecting magnetic field is in the L-direction, and is the direction of maximum variance in $\boldsymbol{B}$ over the time interval from 5:03:56.5 to 5:03:57.2 UT (between the vertical dotted lines) [26]. The minimum variance direction, *N*, is normal to the reconnecting current sheet. The intermediate variance direction, *M*, is the direction of the guide field and Hall magnetic field perturbations [e.g. 27]. The directions of *L*, *M*, and *N* in geocentric solar ecliptic (GSE) coordinates are given in Figure 2. Fig. (1f) shows the measured electric current density, $\boldsymbol{J} = ne(\boldsymbol{V_i} - \boldsymbol{V_e})$, also in LMN coordinates, where *n* is the number density, and *e* is the electron charge.

During the interval shown in Figure (1), there is a slow rotation in B_M from positive to negative. Between the vertical dotted lines, there is a rapid reversal in B_L that coincides with a bipolar perturbation in B_M from the background value, a positive enhancement in B_N and a local minimum in $|\boldsymbol{B}|$, all of which are signatures of a reconnecting current sheet [28]. There is also a significant out of plane current, $J_M \sim 1.8$ μA/m^2. B_L is 20 nT, while the background B_M is approximately 10 nT, giving a guide field of 0.5. The background B_M was nearly flat over the interval where minimum variance analysis was performed. In between the bipolar perturbation in B_M, which corresponds to the Hall magnetic field [28], there is a positive enhancement in V_{eL}, signifying the observation of an electron jet on the +L side of the ion diffusion region [6]. Because there is only a weak positive perturbation in V_{iL}, and there are adequate ion measurements to produce moments, the ion jet had likely not fully formed, suggesting the spacecraft was close to the EDR. The V_{eL} jet occurred close to the center of the current sheet ($B_L=0$, vertical dashed line) but was slightly offset from the minimum in B and $B_L=0$, which is consistent with previous observations [29] and simulations showing the distortion of the quadrupolar Hall magnetic field signature by the guide field [20, 30, 31, 32, 33]. The V_{eL} jet therefore carries a current in the -*L* direction of ~0.5 μA/m^2, which is partially aligned with $\boldsymbol{B}$.

Panel (g) shows the measured $E_{\|}$ with a measurement uncertainty of ~1 mV/m, as well as the perpendicular electric field, E_{perp}, transformed into the frame of the ion bulk flow by calculating $(\boldsymbol{E}'_{ion} = \boldsymbol{E} + \boldsymbol{V}_i \times \boldsymbol{B})$. At the time the electron jet is observed, there is an $E_{\|}$ of -4 mV/m, which could contribute to the acceleration of the electron jet. E_{perp} is also enhanced, suggesting an oblique electric field structure. Finally, panel (h) shows the dissipation, $\boldsymbol{J} \cdot \boldsymbol{E}'$, in the electron frame of reference. Contributions to $\boldsymbol{J} \cdot \boldsymbol{E}'$ from electric fields parallel and perpendicular to $\boldsymbol{B}$ are color coded, with labels on the right of the figure. There is an enhancement of $\boldsymbol{J} \cdot \boldsymbol{E}' = 8$ nW/m^3 which is comparable to dissipation observed in the EDR by MMS in asymmetric reconnection at the dayside magnetopause [16, 17, 18, 30]. The dissipation is largely due to $E_{||}$.

Similar features to those shown in Figure (1) were seen on all four spacecraft, and are shown in Figure (2). Panels (a) and (b) shows the reversal in B_L and the bipolar Hall B_M signature, respectively. MMS2 and MMS4 see the weakest hall signatures, while MMS1 and MMS3 see the largest. Panel (c) shows the $E_{\|}$ measured at 8192 samples/s for all four spacecraft, with the zero line offset by multiples of 5 mV/m to make each signal visible. A similar $E_{\|}$ signal is seen for all four spacecraft, with varying amplitudes. MMS2 observes the weakest $E_{\|}$ at -3 mV/m, while MMS3 sees the strongest at -5 mV/m. Additionally, on the $+B_L$ side of the current sheet, higher frequency $E_{\|}$ waves are observed that include bipolar electrostatic solitary waves (ESWs) with positive-to-negative polarity. These ESWs are consistent with electron holes generated by a streaming instability associated with a negative $E_{\|}$ accelerating electrons along $\boldsymbol{B}$ [34]. Panel (d) shows $\boldsymbol{J} \cdot \boldsymbol{E}'$, with the weakest values again observed on MMS2 and the largest on MMS3. Panel (e) shows the barycentric $\boldsymbol{E}'$ calculated using all four spacecraft and the electric field due to the

divergence of the electron stress tensor, $\boldsymbol{E}_{\nabla\cdot\boldsymbol{T}} = -\nabla\cdot\overleftrightarrow{\boldsymbol{T}}/ne$, where $\overleftrightarrow{\boldsymbol{T}} = m_e\int \boldsymbol{v}\boldsymbol{v}f_e\, d^3v = \overleftrightarrow{\boldsymbol{P}}_{\boldsymbol{e}} + nm_e\boldsymbol{V}_e\boldsymbol{V}_e$, f_e is the electron phase space distribution measured by FPI, and $\overleftrightarrow{\boldsymbol{P}}_e$ is the electron thermal pressure. The contribution to $\boldsymbol{E}'$ due to inertia, $\boldsymbol{E}_{(\boldsymbol{V}\cdot\nabla)\boldsymbol{V}} = -m_e(\boldsymbol{V}_e\cdot\nabla)\boldsymbol{V}_e]/e$, is also shown. Note that the different electric fields are slightly offset in time, due to the fact that the spacecraft are observing a structure that may vary on spatial scales smaller than the spacecraft separation, leading to down-sampling of the structure and temporal offsets. $\boldsymbol{E}'$ is near zero throughout the plotted interval, as expected for frozen-in electrons, except in the electron jet region, where there is an enhancement in the L and M components. This enhancement coincides with an enhancement in $\boldsymbol{E}'_{\nabla\cdot\boldsymbol{T}}$. Because the inertial term remains near zero, the parallel electric field is balanced by an electron pressure divergence, similar to results from laboratory experiments for guide field reconnection [35].

A significant $E_\parallel$ in the electron jet that acts to accelerate electrons is a novel observation in space plasmas. Fig. (2f) shows the configuration of the four spacecraft in LMN coordinates. MMS2 observes the current sheet first, followed by MMS3, and then MMS1 and MMS4 nearly simultaneously. This is consistent with a current sheet being carried by the magnetosheath bulk flow, which is mostly in the -*N* and -*M* directions. The separation of the spacecraft along the *L* direction suggests that MMS2 and MMS4 were closest to the EDR, MMS3 was farthest along the electron jet, and MMS1 was intermediate between the three. From multi-spacecraft timing [36], the reconnecting current sheet moved at a speed between 100 and 150 km/s, suggesting a width of the Hall perturbations of 25-38 km, which is less than the ion skin depth in this case (~50 km) and is indicative of the spacecraft being near the EDR. Comparing the formation with the top of Fig. (2) shows that $E_\parallel$ and its associated dissipation persists with increasing distance along *L*. The four spacecraft encounter the $E_\parallel$ over 200 ms (~10,000 electron plasma periods), which means it is a temporally persistent spatial structure. The structure is significantly larger than the Debye length, which is 10s of meters in this case, and because it is observed on all four spacecraft, it likely extends beyond the spacecraft separation, which is ~10 km.

Figure 2. Data from all four spacecraft. (a) B_L. (b) B_M. (c) $E_\parallel$ measured at 8192 samples/s. (d) $\boldsymbol{J}\cdot\boldsymbol{E}'$. (e) L and M components (offset by 2 mV/m) of barycentric $\boldsymbol{E}'$ as well as $\boldsymbol{E}_{\nabla\cdot\boldsymbol{T}}$ and $\boldsymbol{E}_{(\boldsymbol{V}\cdot\nabla)\boldsymbol{V}}$ (f) Spacecraft formation plot in LMN-coordinates with MMS1 at the origin and larger circles representing positive M.

Figure (3a) shows a schematic of the reconnecting current sheet, as well as the normal motion of the four MMS spacecraft as they encounter it. All four spacecraft observed the electron jet and skewed bipolar Hall magnetic fields due to the guide field. This skewed Hall magnetic field led to the jet being directed toward the $+B_L$ side of the current sheet, leading to a component of $\boldsymbol{V}_e$ along $\boldsymbol{B}$. MMS2 and MMS4 encountered the current sheet closest to the EDR, and MMS3 was the furthest along the electron jet. $E_\parallel$ appeared to grow along the jet, and it is not clear how far past the position of MMS3 this trend continued.

Figure 3. (a) A schematic of the observed current sheet with the MMS normal spacecraft tracks inferred from **B,** $E_{||}$, V_{eL} and the time delays from all MMS spacecraft. Solid lines indicate the magnetic field lines, and dashed lines indicate the separatrix. Yellow indicates regions of Hall magnetic field perturbations. Note that the electron jet and $E_\parallel$ at

least partially overlap. (b) A schematic of the $E_{\|}$ within an oblique acceleration channel. Dashed lines are the width of the channel, the black arrow is the magnetic field vector, the blue arrow is the parallel electron flow, and the red arrow is $E_{\|}$. Note that the orientation of **B** in the LMN coordinate system is changing across the channel.

III. ELECTRON DISTRIBUTIONS

All four spacecraft observe similar features in the electron distributions in the vicinity of the $E_{\|}$ structure. Figure (4) shows 2-D parallel slices of the distributions from MMS1 as a representative example for three times near the peak value of $E_{\|}$. Figure (4a) shows the distribution at 05:03:56.782 UT before the spacecraft observes enhanced $E_{\|}$, which is on the –N side of the structure. The distribution is fairly close to isotropic and Maxwellian. Figure (4b) shows the distribution at 05:03:56.872 UT, which is nearest to the peak $E_{\|}$. At this time, there is significant parallel heating as well as acceleration in the parallel direction. Figure (4c) shows the distribution on the +N side of the $E_{\|}$ structure measured at 05:03:56.932 UT. At this point, the parallel heating of the distribution persists, and there is an enhanced anti-parallel population. Similar distributions were observed throughout the interval where waves and ESWs were observed. The fact that heated electrons are only seen on one side of the $E_{\|}$ suggests that the electrons are entering on the -N side of the structure and exiting on the +N side, which is consistent with the structure being oblique to the background magnetic field. This is also consistent with the waves and ESWs only being seen on the +N side for all four spacecraft, shown in Figure (2c). Additionally, there's very little evidence of significant acceleration along the +L direction when comparing parallel slices between MMS1, 3, and 4, which is consistent with electrons being accelerated through the oblique channel as opposed to along it.

The particle and electric field observations are consistent with electrons traversing through an oblique "acceleration channel" with a significant $E_{\|}$. A schematic of such a channel is shown in the frame of the rapidly varying magnetic field in Figure (3b). The electrons enter the channel on one side, experiencing both a parallel and perpendicular electric field. This results in electron heating and acceleration. When the electrons exit, a streaming instability develops near the jet, associated with electron phase space holes that act to create a reflected anti-parallel population and maintain the heated distribution. This explains why, in Figure (1c), enhanced $T_{e\|}$ extends past the region of peak $\boldsymbol{J} \cdot \boldsymbol{E}'$, skewed toward the region where B_L is positive.

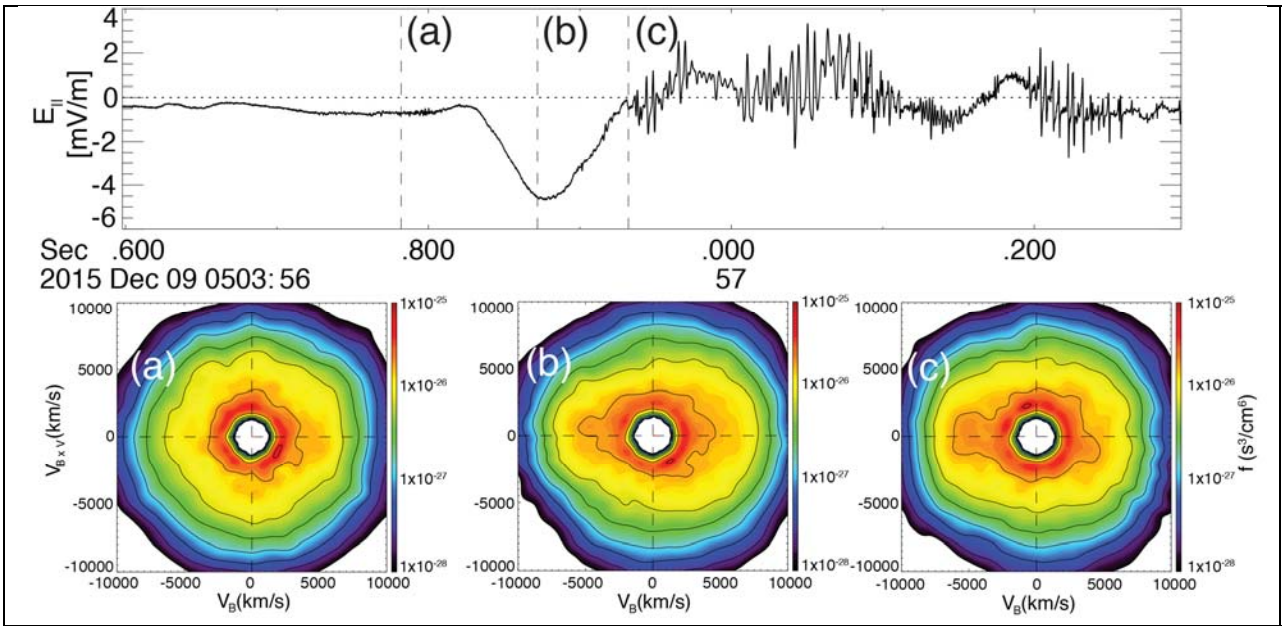

Figure 4. (Top) $E_{||}$ from MMS1. Vertical lines correspond to three electron distributions collected (a) before the observed $E_{||}$, (b) at the time of peak $E_{||}$, and (c) when $E_{||}$ returns to zero and the instability begins. The abscissa for the distributions corresponds to velocities along the **B** ($V_{\mathbf{B}}$) and the ordinate corresponds to velocities along the E_{perp} direction ($V_{\mathbf{B}\times\mathbf{V}}$).

IV. DISCUSSION AND CONCLUSIONS

The observations indicate that all four spacecraft encountered the electron jet of symmetric reconnection under a moderate guide field. The electron jet was skewed towards the separatrix on the positive B_L side of the current sheet, consistent with a distorted Hall magnetic field signature, and therefore carried a significant current along $\boldsymbol{B}$. A persistent $E_{||}$ of 3-5 mV/m was observed coincident with the jet, leading to significant ($\boldsymbol{J}\cdot\boldsymbol{E}'$) nearing 8 nW/m^3 across the spacecraft constellation.

These results have several important implications for understanding the conversion of electromagnetic energy into particle kinetic energy and heat by magnetic reconnection. First, this specific $E_{||}$ signature in the electron jet has not been reported before in either space-based observations or 2D simulations. Second, the fact that the $E_{||}$ was associated with significant ($\boldsymbol{J}\cdot\boldsymbol{E}'$) suggests that, in addition to the EDR, the electron jet contributes to extended dissipation of electromagnetic energy into electron kinetic energy and heat. This may be unique to guide-field magnetic reconnection, as the Hall fields skew the electron jet to have a component along **B**. Finally, there is evidence that the electric field structure is oblique and that it acts as an acceleration channel that heats electrons passing through it in the electron jet. Further theory and simulations will be needed to determine if this acceleration channel is an effect of the guide field.

ACKNOWLEDGEMENTS

This work was funded by the NASA MMS project. The authors recognize the tremendous effort in developing and operating the MMS spacecraft and instruments and sincerely thank all involved.

REFERENCES

[1] B. U. O□. Sonnerup, *et al*., *J. Geophys. Res*., **86**, 10049–10067 (1981).
[2] S. Masuda, T. Kosugi, H. Hara, S. Tsuneta, Y. Ogawara, *Nature*, **371**, 495-497 (1994).
[3] F. S. Mozer, S. D. Bale, and T. D. Phan, *Phys. Rev. Lett.*, **89**, 015002 (2002).
[4] P. Louarn, *et al.*, *Geophys. Res. Lett.*, **31**, L19805 (2004).
[5] J. T. Gosling, R. M. Skoug, D. J. McComas, and C. W. Smith, *J. Geophys. Res*., **110**, A01107 (2005).
[6] T. D. Phan, J. F. Drake, M. A. Shay, F. S. Mozer, and J. P. Eastwood, *Phys. Rev. Lett.*, **99**, 255002 (2007).
[7] G. Paschmann, M. Øieroset, and T. Phan, *Space Sci. Rev.*, **178** (2–4), 385–417 (2013).
[8] D. A. Uzdensky, B. Cerutti, and M. C. Begelman, *Astrophys. J. Lett.,* **737**, L40 (2011).
[9] J. Egedal, W. Fox, N. Katz, M. Porkolab, K. Reim, and E. Zhang, *Phys. Rev. Lett.,* **98**, 015003 (2007).
[10] G. Paschmann, *et al*., *Nature*, **282**, 243–246 (1979).
[11] J. L. Burch, and J. F. Drake, *Am. Sci.,* **97**, 392–399 (2009)
[12] M. Hesse, T. Neukirch, K. Schindler, M. Kuznetsova, and S. Zenitani, *Space Sci. Rev.*, **160**, 3–23 (2011).
[13] J. L. Burch, T. E. Moore, R. B. Torbert, and B. L. Giles, *Space Sci. Rev*., **199**, 5-21 (2016).
[14] J. R. Shuster, L.-J. Chen, M. Hesse, M. R. Argall, W. Daughton, R. B. Torbert, and N. Bessho, *Geophys. Res. Lett.*, **42**, 2586–2593 (2015).
[15] L.-J. Chen, M. Hesse, S. Wang, N. Bessho, and W. Daughton, *Geophys. Res. Lett*., **43**, 068243, (2016).
[16] J. L. Burch, *et al.*, *Science*, doi:10.1126/science.aaf2939, (2016).
[17] J. L. Burch and T. D. Phan, *Geophys. Res. Lett.,* **43**, 8327-8338 (2016).
[18] L.-J. Chen et al., *Geophys. Res. Lett.,* **43,** 6036-6043 (2016)
[19] S. Zenitani, M. Hesse, A. Kilmas, M. Kuznetsova, *Phys. Rev. Lett.*, **106**, 195003 (2011)
[20] S. Eriksson, D. L. Newman, G. Lapenta and V. Angelopoulos, *Plasma Phys. Control. Fusion,* **56,** 064008, (2014).
[21] R. B. Torbert, *et al*., *Space Sci. Rev*., **199**, 105-135 (2016).
[22] R. E. Ergun, *et al*., *Space Sci. Rev*., **199**, 167-188 (2016).
[23] P.-A. Lindqvist, *et al.*, *Space Sci. Rev*., **199**, 137-165 (2016).
[24] C. T. Russell, *et al*., *Space Sci. Rev*., **199**, 189-256 (2016).
[25] C. Pollock, *et al*., *Space Sci. Rev*., **199**, 331-406 (2016).
[26] B. U. Ö. Sonnerup, and M. Scheible, Minimum and maximum variance analysis, in *Analysis Methods for Multi-Spacecraft Data,* edited by G. Paschmann and P. W. Daly, *ISSI Sci. Rep., SR-001,* p. 185-220, ESA Publ. Div. Noordwijk, Netherlands (1998).
[27] H. Zhang et al., *J. Geophys. Res.,* doi:10.1029/2007JA012789 (2016).
[28] F. S. Mozer, S. D. Bale, and T. D. Phan, *Phys. Rev. Lett.,* **89**, 015002-4 (2002).

[29] J. P. Eastwood, M. A. Shay, T. D. Phan, and M. Øieroset, *Phys. Rev. Lett.,* **104**, 205001 (2010).
[30] S. Eriksson et al., *Phys. Rev. Lett.,* **117**, 015001 (2016).
[31] A. G. Frank et al., *Phys. Lett. A,* **348,** 318 (2006).
[32] T. D. Tharp et al., *Phys. Rev. Lett.,* **109**, 165002 (2012)
[33] A. Le et al., *Phys. Rev. Lett.,* **110,** 135004 (2013).
[34] R. E. Ergun et al., *Phys. Rev. Lett.,* **102**, 155002 (2009).
[35] W. Fox et al., *Phys. Rev. Lett*., **118**, 125002 (2017).
[36] S. J. Schwartz, Shock and Discontinuity Normals, Mach Numbers, and Related Parameters, in *Analysis Methods for Multi-Spacecraft Data,* edited by G. Paschmann and P. W. Daly, *ISSI Sci. Rep., SR-001,* p. 249-270, ESA Publ. Div. Noordwijk, Netherlands (1998).

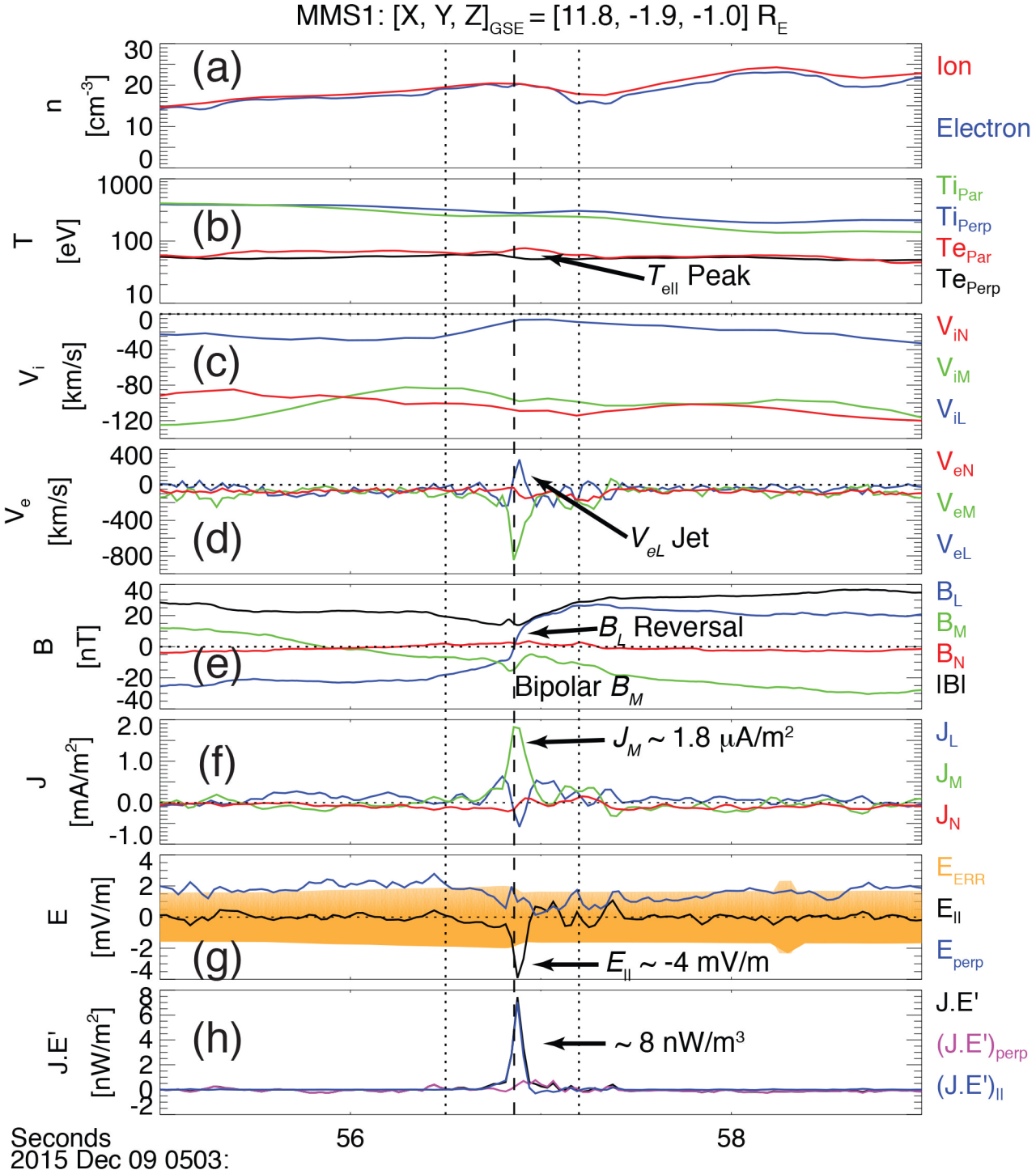
MMS1: [X, Y, Z]GSE = [11.8, -1.9, -1.0] RE
(a)
n [cm-3]
30
20
10
0
Ion
Electron
(b)
T [eV]
1000
100
10
TiPar
TiPerp
TePar
TePerp
Tell Peak
(c)
Vi [km/s]
0
-40
-80
-120
ViN
ViM
ViL
(d)
Ve [km/s]
400
0
-400
-800
VeN
VeM
VeL
VeL Jet
(e)
B [nT]
40
20
0
-20
-40
BL
BM
BN
IBI
BL Reversal
Bipolar BM
(f)
J [mA/m2]
2.0
1.0
0.0
-1.0
JL
JM
JN
JM ~ 1.8 μA/m2
(g)
E [mV/m]
4
2
0
-2
-4
EERR
E||
Eperp
E|| ~ -4 mV/m
(h)
J.E' [nW/m2]
8
6
4
2
0
-2
J.E'
(J.E')perp
(J.E')||
~ 8 nW/m3
Seconds
2015 Dec 09 0503:
56
58

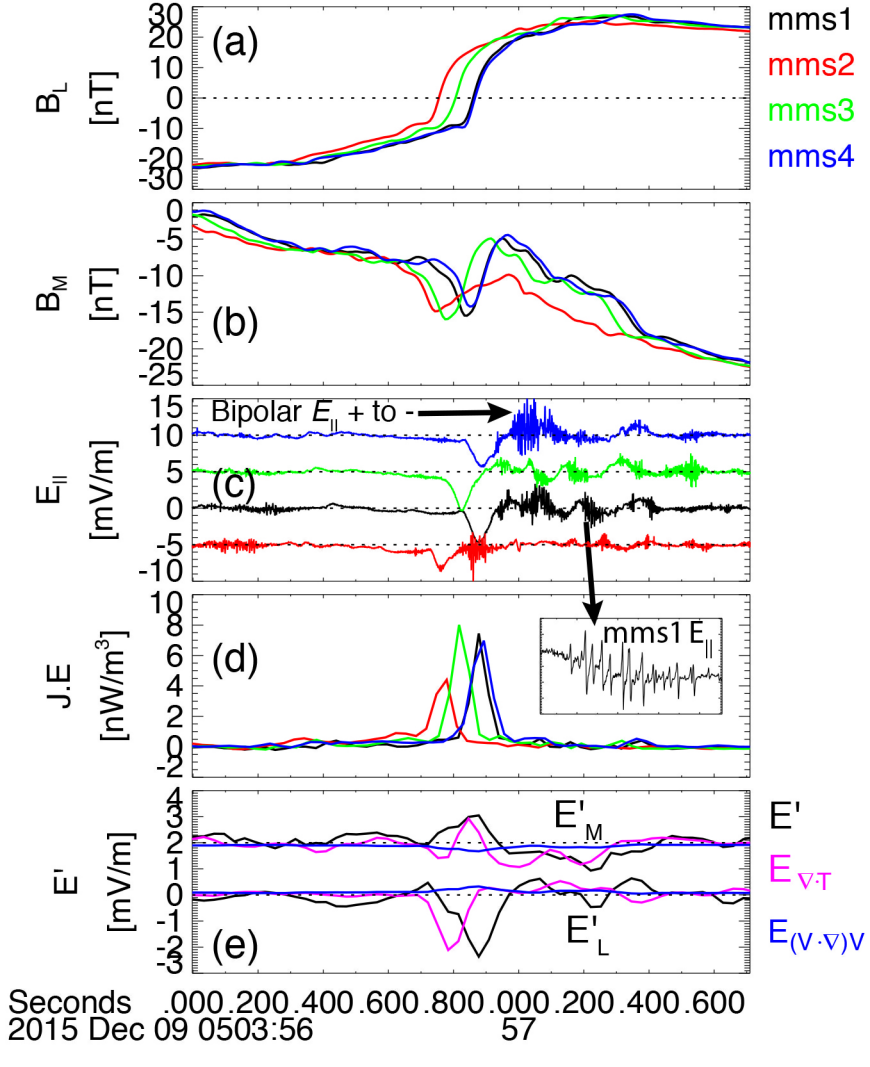
(a)
B_L [nT]
mms1
mms2
mms3
mms4
(b)
B_M [nT]
(c)
Bipolar $E_{||}$ + to -
$E_{||}$ [mV/m]
(d)
mms1 $E_{||}$
J.E [nW/m^3]
(e)
E'
E'_M
E'_L
[mV/m]
$E_{\nabla\cdot T}$
$E_{(V\cdot\nabla)V}$
Seconds .000.200.400.600.800.000.200.400.600
2015 Dec 09 0503:56 57

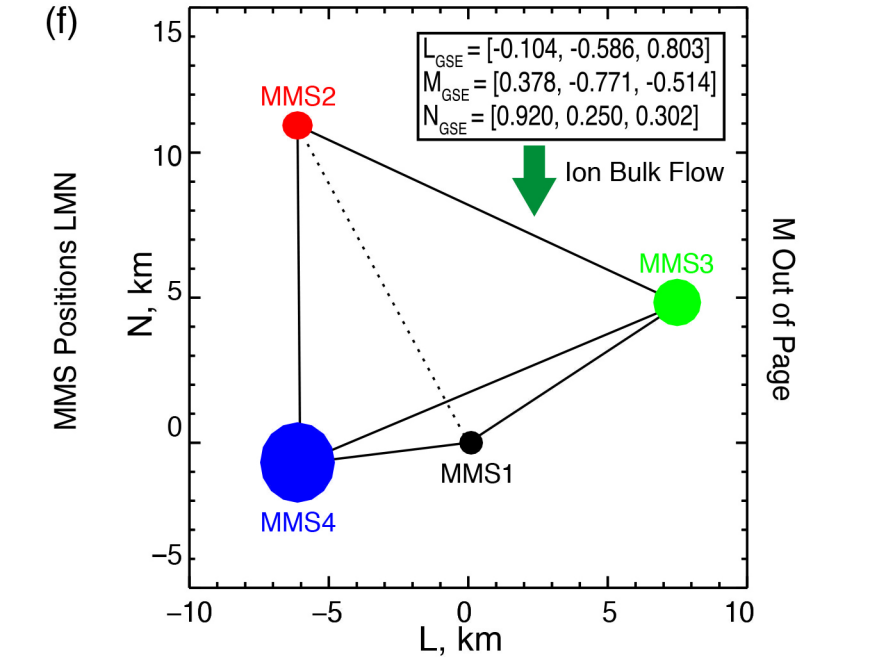
(f)
L_{GSE} = [-0.104, -0.586, 0.803]
M_{GSE} = [0.378, -0.771, -0.514]
N_{GSE} = [0.920, 0.250, 0.302]
Ion Bulk Flow
MMS2
MMS3
MMS1
MMS4
MMS Positions LMN
N, km
L, km
M Out of Page

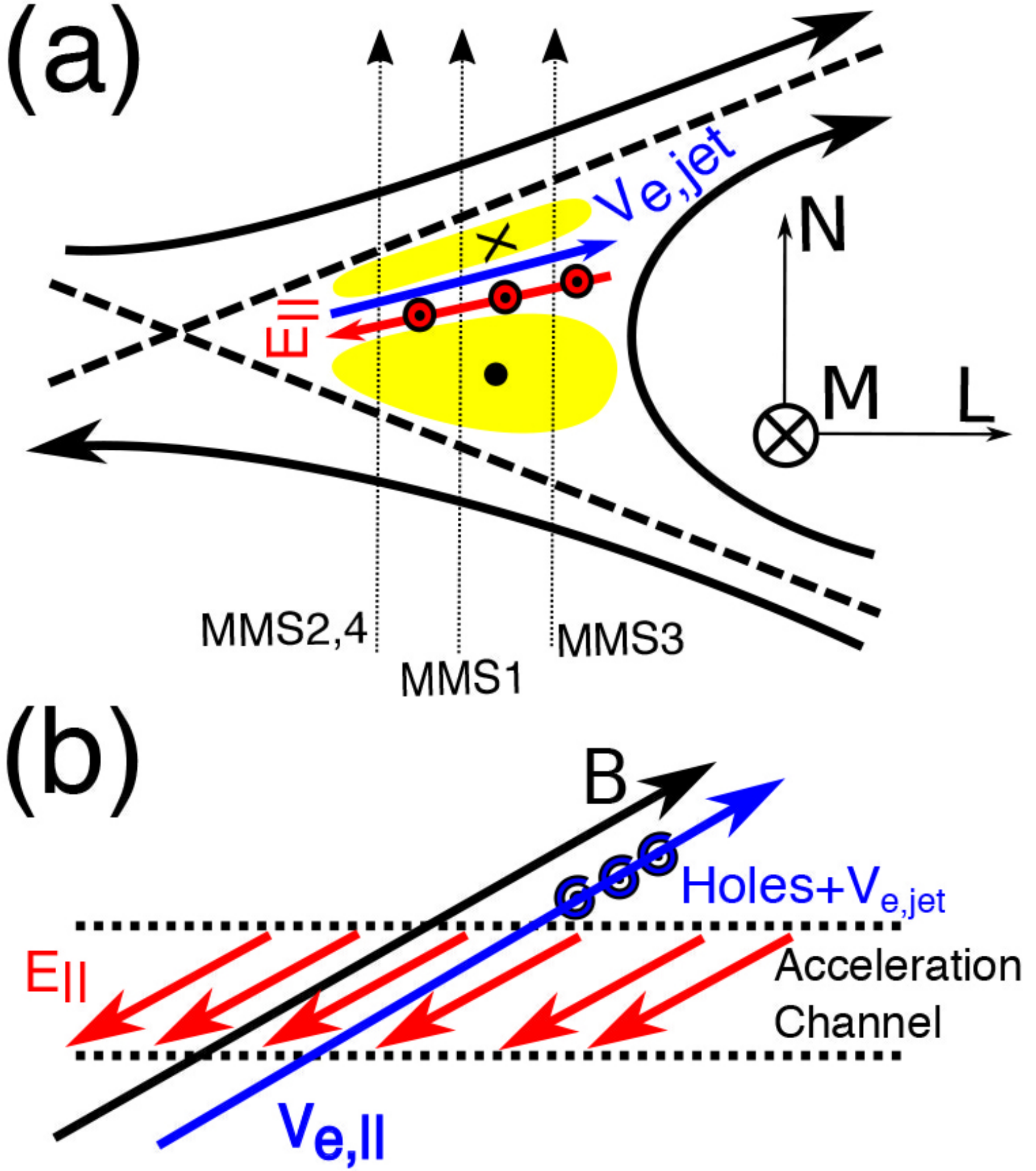
(a)
Ve,jet
E||
N
M
L
MMS2,4
MMS1
MMS3
(b)
B
Holes+Ve,jet
E||
Acceleration
Channel
Ve,||

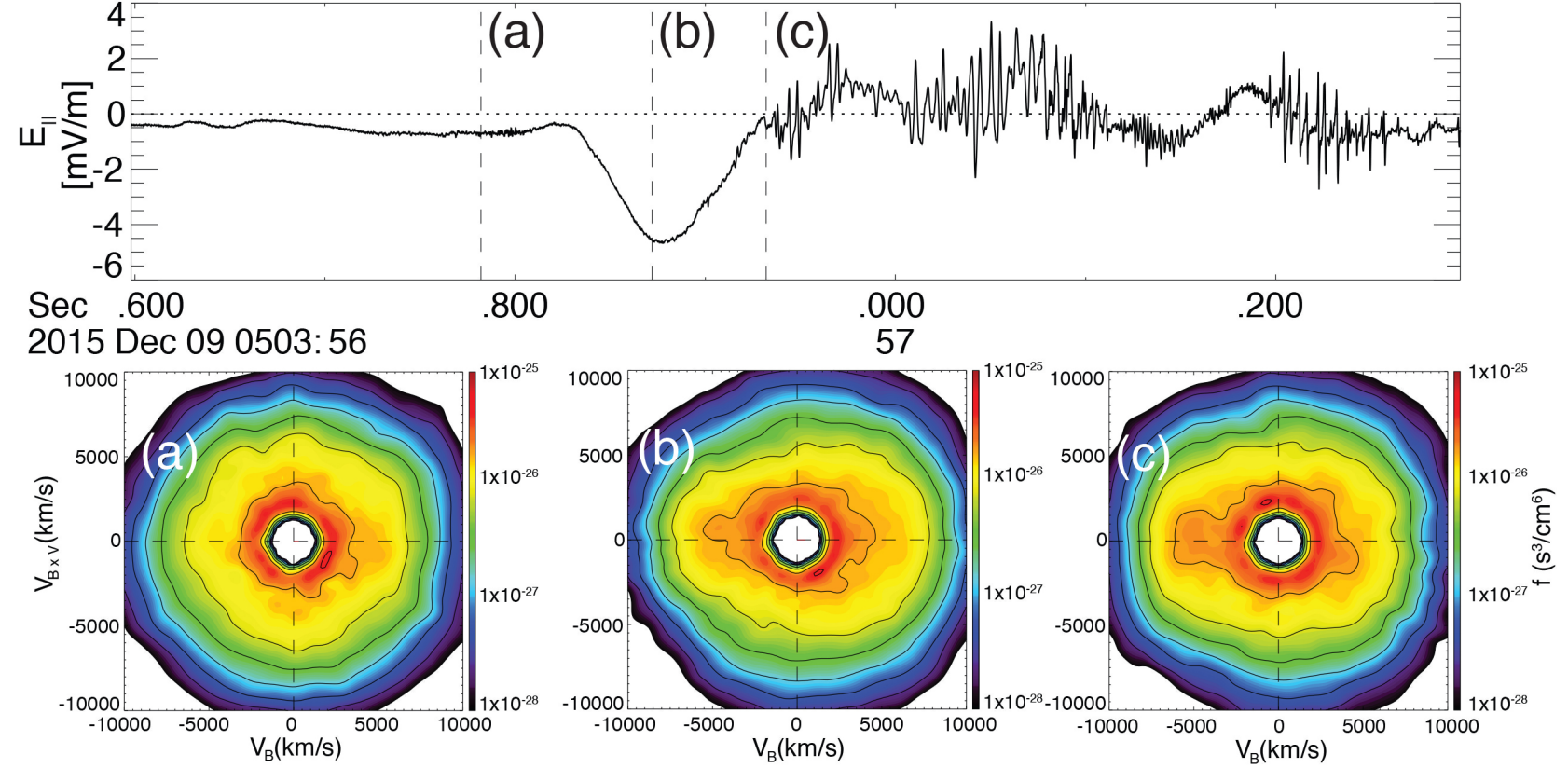
(a)
(b)
(c)
$E_{||}$ [mV/m]
4
2
0
-2
-4
-6
Sec .600
.800
.000
.200
2015 Dec 09 0503:56
57
$V_{B\times V}$(km/s)
V_B(km/s)
10000
5000
0
-5000
-10000
1x10^{-25}
1x10^{-26}
1x10^{-27}
1x10^{-28}
f (s^3/cm^6)